

Mechanical modeling of CNT structures

Part I: Introduction

Fernando Fraternali
University of Salerno

Workshop
Carbon nanotubes as components in bulk materials
University of Salerno
October 25 - November 04, 2011

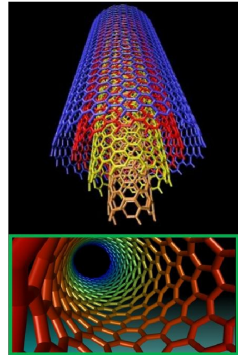
- 1 Background
- 2 Motivation
- 3 Lecture overview

Background on CNTs

Basic facts

CNTs have been proposed for a **number of applications**.

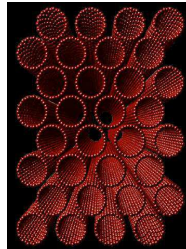
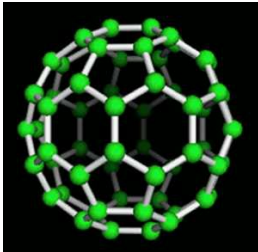
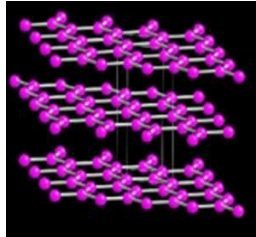
- Discovered in 1991 by Iijima;
- **Single-walled** or **multi-walled**;
- Nearly one-dimensional structures;
- **Unique material properties:**
 - Exceptional Mechanical Strength
 - Low Density
 - Exceptional Current Carrying Capacity
 - Exceptional Heat Transmission
 - Exceptional Temperature Stability
 - Chemically Stable



Mechanical response and bending/buckling modes of CNTs under **axial** and **radial deformation** have been studied using **experimental**, **theoretical** and **molecular-dynamics** analysis.

Background on CNTs

Carbon allotropes (diamond, graphite, buckyballs and carbon nanotubes)



Background on CNTs

Experimental findings 1/4

Elastic modulus $E \sim 1 \text{ TPa}$ (Pantano et al., 2004).

In experiments this value can vary widely, depending on:

- the number of defects,
- the CNT microstructure,
- the synthesis method.

CNT based structures exhibit a **super-compressible foam-like behaviour** (Gibson and Ashby, 1999), with marked **hysteresis** and the **alternation of three distinct regimes**:

- linear elastic response for small strains,
- a plateau region associated with buckling for intermediate strains,
- a densification regime for high strains.

Background on CNTs

Experimental findings 2/4

The material also shows **remarkable fatigue resistance** when synthesised with catalyst coating techniques, able to be repeatedly compressed to large strains ($\epsilon \geq 0.8$) and to still show **significant recovery** and **dissipative effects** in subsequent compressive cycles (Suhr et al., 2007).

As aligned arrays of CNTs are compressed the strain is preferentially **localised at their base** (Cao et al., 2005).

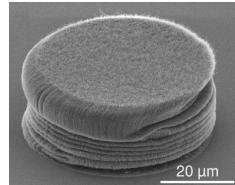
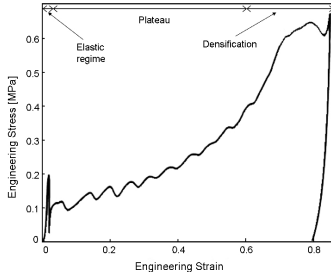
This is thought to be a result of a **gradient in density along the height**, increasing from the base to the top (Hutchens et al., 2010). Such graded properties are known to have important effects on certain mechanical properties such as:

- failure resistance,
- impact absorption.

Background on CNTs

Experimental findings 3/4: compression of carbon nanotube bundles

In situ uniaxial compression experiments have shown **bottom-to-top sequential buckling**, which produce **gradual collapse** of the structure. The buckling regime features characteristic **stress humps** and **strain bursts**.

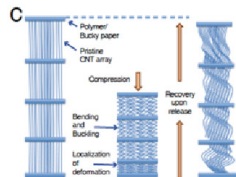
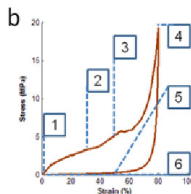
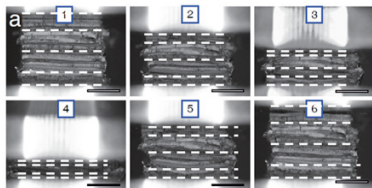


From Hutchens et al., Adv. Funct. Mater., 20:1-9, 2010.

Background on CNTs

Experimental findings 4/4: compression of multilayered CNT foams

Experimental studies on multilayer CNT assemblies have demonstrated that such structures exhibit **superior dissipation performance**, as compared to their single layer counterparts.



movie >

Courtesy of Abha Misra, Luigi De Nardo, Jordan R. Raney, Anna Craig and Chiara Daraio, California Institute of Technology.

Background on CNTs

Available mechanical models

Both **theoretical** and **numerical approaches** have been proposed in the literature.

We can distinguish two main categories:

Molecular Dynamics models (MD)

- show that the NT walls can be accurately treated as elastic shells if the elastic moduli and thickness are properly assigned;
- less practical in investigating the behaviour of long CNTs, MWCNTs, and CNT bundles involving a large number of atoms (due to the limitation in time and length scales).

Continuum Mechanics models (CMMs)

- can be derived applying the Cauchy-Born rule, which relates the deformation of a lattice structure (or crystal) to that of continuous medium (Ericksen, 2008).
- The elastic potential is obtained by matching the energy of a representative cell of the crystal to that of an equivalent volume of continuous medium.
- The resulting constitutive model only relies on atomistic properties, and does not require phenomenological input.

The mechanical modelling of **CNT structures** naturally involves **different length scales**, including

- **Microscale**: scale of individual carbon atoms or groups of atoms (coarse-graining);
- **Mesoscale**: scale of repetitive assemblies of microscopic structures;
- **Macroscale**: scale of the entire structure.

It is therefore essential to model the mechanical behaviour of such structures through reliable **scale bridging approaches** (refer, e.g., to by (Müller et al., 2006), (Tu and Ou-Yang, 2008)).

Lecture overview 1/3

On the basis of previous discussions and with the aim to formulate a **general variational framework** for the **mechanical analysis** of **CNT structures** at **different scales**, we deal in the present lecture with the following tasks:

- multiscale modelling of **hysteresis** and **strain localisation** in **nanoparticle lattices** endowed with **bistable elastic potentials**;
- **mechanical modelling** and **structural identification** of **CNT foams** and **CNT multilayer assemblies**.

A rational approach to the limiting energies at the mesoscopic scale energies consists of determining the **continuum limits** of the **discrete interaction potentials**, which characterize the microscopic response (**bistable elastic potentials**).

Lecture overview 2/3

Multiscale models of CNT structures

We formulate a **multiscale mechanical model** of **CNT structures** under **compressive loading**, which is inspired by some distinctive features of the **micromechanical response** reported earlier in the literature for such materials (see, e.g., Cao et al., 2005; Hutchens et al., 2010)

The given model make uses of **multiscale chains** of **lumped masses** connected by **nonlinear springs**, and captures the characteristic **'three-phase'** response of the examined structures (a:**linear response**; b:**buckling**; c:**densification**).

We show that a series of bistable elastic springs indeed exhibits such a kind of response, and through-the-thickness **localisation** of the **axial deformation**, mimicking the **snap-buckling** events and the **macroscopic hysteresis** observed in real CNT arrays.

Lecture overview 3/3

'In situ' parameter identification of CNT structures

We present an '*in situ*' identification procedure to experimentally determine the material constants that characterise the response of CNT multilayer structures.

To directly extrapolate material parameters, we inspect the local axial deformation of the CNTs through the thickness of a multilayer structure during collapse. We show that the proposed CNT model can be used to capture the local response at multiple length scales (through high resolution cameras, SEM tools, etc.).

This allows a first experimental approximation of the mechanical parameters, which can be effectively used to run a successive parameter optimisation procedure.

Mechanical modeling of CNT structures

Part II: Multiscale models and parameter identification

Fernando Fraternali
University of Salerno

Workshop
Carbon nanotubes as components in bulk materials
University of Salerno
October 25 - November 04, 2011

Outline

- 1 Introduction
- 2 The mechanical model at the microscopic scale
- 3 Dynamic relaxation and hysteresis at the mesoscale
- 4 Multiscale numerical modeling
- 5 Applications
 - Convergence study
 - Simulation of experimental results on compressed CNT foams
- 6 Multilayer CNT structures
 - Mechanical modelling of multilayer CNT structures
 - *In situ* parameter identification
 - Numerical examples

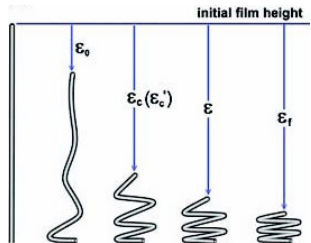
The present part of this Thesis is devoted to the formulation of **multiscale models of CNT structures** based on **lattices of bistable elastic springs**.

Mechanical models consisting of chains of bistable springs have been proposed and extensively studied by several authors for different scopes (refer e.g. to Puglisi and Truskinovsky, 2005). The essential feature of a bistable spring consist of the fact that its equilibrium path encompasses **two (stable) elastic phases** (say **phases a and b**), with interposed an **(unstable) spinodal regime (phase c)**.

Such a peculiar response is able to describe relevant material behaviours, like, e.g., **martensitic phase transformations** and **transformational plasticity**, through the **interplay** between **macroscopic** and **microscopic length scales**.

In particular, we show in this study that **multiscale models of bistable springs** are capable to describe some relevant features of the experimentally observed **micromechanical behaviour** of **CNT arrays** under **compression tests**.

The latter is characterized by a succession of **inhomogeneous equilibrium configurations** (due to **progressive CNT kinking**) and **macroscopic hysteresis** (induced by **friction**, **entanglement** of the tubes and other **dissipative effects**).



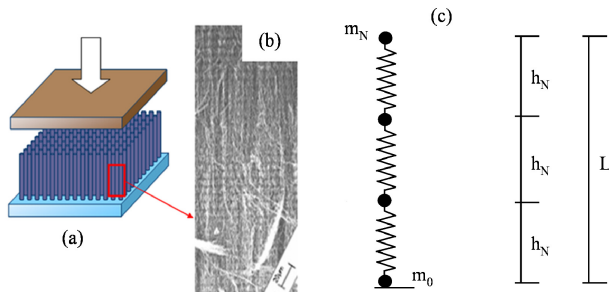
(From Cao et al., Science, 2005)

The modelling proposed in the present study introduces **three different length scales**:

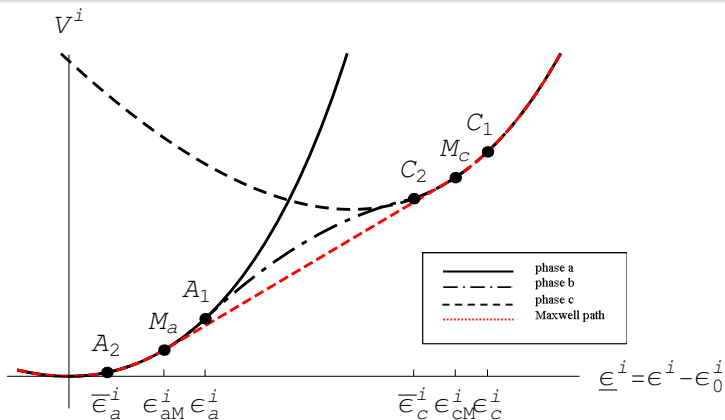
- Microscale (10^{-9} m) : individual bistable springs, representing **infinitesimal portions** of the **CNT structure**;
- **Mesoscale** (10^{-6} m) : limit of an infinite series of microscopic springs, representing **finite portions** of the **structure**;
- **Macroscale** (10^{-3} m) : **entire structure**.

The mechanical model at the microscopic scale

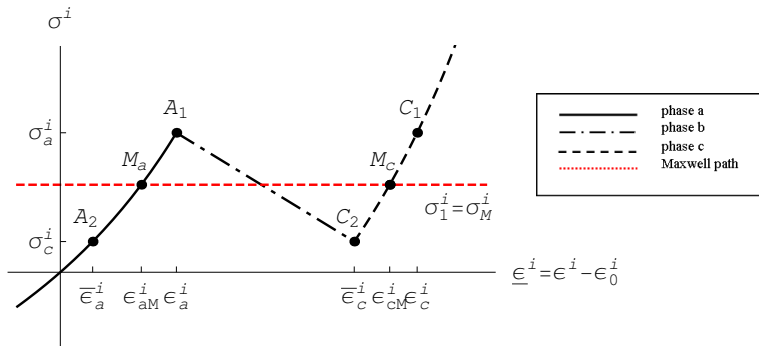
We consider for $N \geq 2$ an infinitesimal portion of a CNT array modeled as a collection of $N + 1$ lumped masses m_0, \dots, m_N piled up one over the other. The nearest neighboring mass points are connected by N microscopic bistable springs.



Mechanical energy V^i of the generic microscopic spring



Stress σ^i versus strain ϵ^i relationship in the generic microscopic spring



movie >

Analytical expression of the stress-strain relationship in the generic microscopic spring (five independent parameters: $k_0^i > 0$, $k_b^i < 0$, $k_c^i > 0$, $\varepsilon_a^i > 0$, and $\bar{\varepsilon}_c^i \geq \varepsilon_a^i$)

$$\sigma^i(\underline{\varepsilon}^i) = V^{i'} = \begin{cases} k_0^i \frac{\underline{\varepsilon}^i}{1 - \underline{\varepsilon}^i}, & \underline{\varepsilon}^i < \varepsilon_a^i \\ \sigma_a^i + k_b^i(\underline{\varepsilon}^i - \varepsilon_a^i), & \varepsilon_a^i \leq \underline{\varepsilon}^i \leq \bar{\varepsilon}_c^i \\ \frac{k_c^i(\underline{\varepsilon}^i - \varepsilon_*^i)}{1 - (\underline{\varepsilon}^i - \varepsilon_*^i)}, & \bar{\varepsilon}_c^i < \underline{\varepsilon}^i \end{cases} \quad (1)$$

with $\underline{\varepsilon}^i = \varepsilon^i - \varepsilon_0^i$, where $\varepsilon^i = \frac{u_N^i - u_N^{i+1}}{h_N}$ is the total strain, and ε_0^i is an 'initial' (permanent) strain.

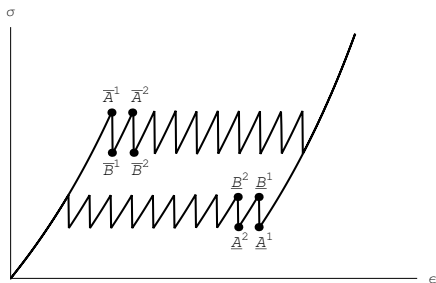
Dynamic relaxation and hysteresis at the mesoscale

We refer the following analysis to a finite portion of a CNT foam, which is modeled as a chain of N identical microscopic springs.

Allowing for dynamic relaxation, we introduce two different time scales:

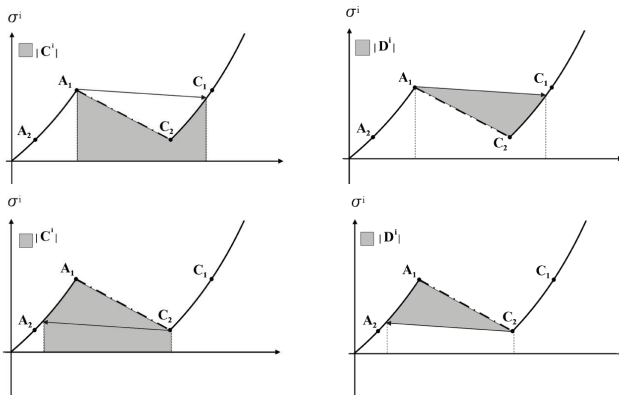
- an external (slow) time $\tau \in [\tau_0, \tau_1]$ ruling an evolution law of the overall deformation ε of the chain;
- and an internal (fast) time $t \in [t_0, t_1]$ governing the microscopic dynamic relaxation for fixed τ

For a given N , a double time integration (with respect to t and τ) produces the following 'sawtooth' response of the system

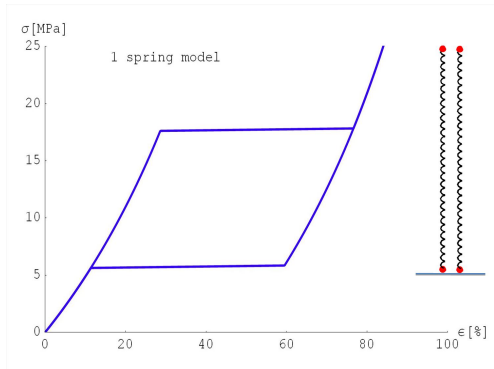


- *elastic steps*
: $\bar{B}^i \rightarrow \bar{A}^{i+1}$
- *plastic steps*
: $\bar{A}^i \rightarrow \bar{B}^i$

movie >

Cold work C^i and dissipated energy D^i in the generic spring

The local 'snaps' $\varepsilon_{C_1}^i - \varepsilon_{A_1}^i$ and $|\varepsilon_{A_2}^i - \varepsilon_{C_2}^i|$ are equal to ε_*/N .



movie > Limiting 'perfectly plastic' response at the mesoscopic scale (transformational plasticity).

Multiscale numerical modeling

We now introduce a multiscale numerical model of a nonlinear mass-spring chain, where each spring represents either a microscopic bistable element or a mesoscopic dissipative element.

As before, we introduce an external (slow) time $\tau \in [\tau_0, \tau_1]$, and an internal (fast) time $t \in [t_0, t_1]$.

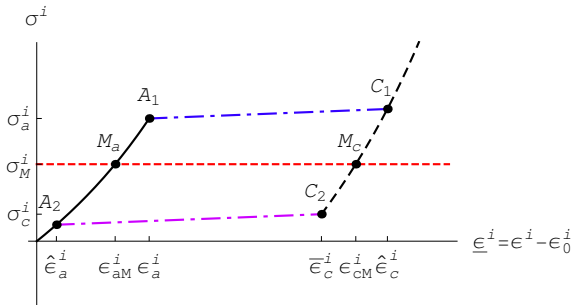
Depending on the adopted model for the individual springs, we may have the t corresponds to the microscopic timescale and τ to the mesoscopic time (*micro-meso transition*), or, alternatively, that t corresponds to the mesoscopic time and τ to the macroscopic time (*meso-macro transition*).

We introduce a discretization $\{\tau_1, \dots, \tau_M\}$ of the loading interval $[\tau_0, \tau_1]$, and compute the system response for fixed $\tau = \tau_k$ through integration with respect to the internal t of the evolution equations

$$m^i \ddot{\hat{u}}_N^i + \gamma^i \dot{\hat{u}}_N^i = \sigma^{i+1} - \sigma^i, \quad i = 1, \dots, N, \quad (2)$$

- $\hat{u}_N^i = \hat{u}_N^i(t)$: transient displacement histories of the masses m_0, \dots, m_N at fixed τ
- *superimposed dots*: derivatives with respect to t
- σ^i : current stresses in the short-range springs
- $\gamma^1, \dots, \gamma^N$: critical damping coefficients

Hardening-type regularization of the mesoscopic response



Analytical expression of the hardening regularization

$$\sigma^i = \begin{cases} \sigma^{(a,i)} = \frac{k_0^i \underline{\varepsilon}_i}{(1 - \underline{\varepsilon}^i)}; (\underline{\varepsilon}^i < \varepsilon_a^i), (\text{flag}^{(k-1)} \neq c) \\ \sigma^{(d,i)} = \sigma_a^i + k_{h+}^i (\underline{\varepsilon}^i - \varepsilon_a^i); (\varepsilon_a^i \leq \underline{\varepsilon}^i \leq \hat{\varepsilon}_c^i), (\text{flag}^{(k-1)} = a) \\ \sigma^{(e,i)} = \sigma_a^i + \Delta \sigma^i + k_{h-}^i (\underline{\varepsilon}^i - \bar{\varepsilon}_c^i); (\hat{\varepsilon}_a^i \leq \underline{\varepsilon}^i \leq \bar{\varepsilon}_c^i), (\text{flag}^{(k-1)} = c) \\ \sigma^{(c,i)} = \frac{k_c^i (\underline{\varepsilon}^i - \varepsilon_*^i)}{1 - (\underline{\varepsilon}^i - \varepsilon_*^i)}; (\bar{\varepsilon}_c^i < \underline{\varepsilon}^i), (\text{flag}^{(k-1)} \neq a) \end{cases} \quad (3)$$

where: $\text{flag}^{(k)} = a$, if $\sigma^i = \sigma^{(a,i)}$; $\text{flag}^{(k)} = c$, if $\sigma^i = \sigma^{(c,i)}$; and $\text{flag}^{(k)} = \text{flag}^{(k-1)}$, otherwise.

Numerical micro-meso convergence study

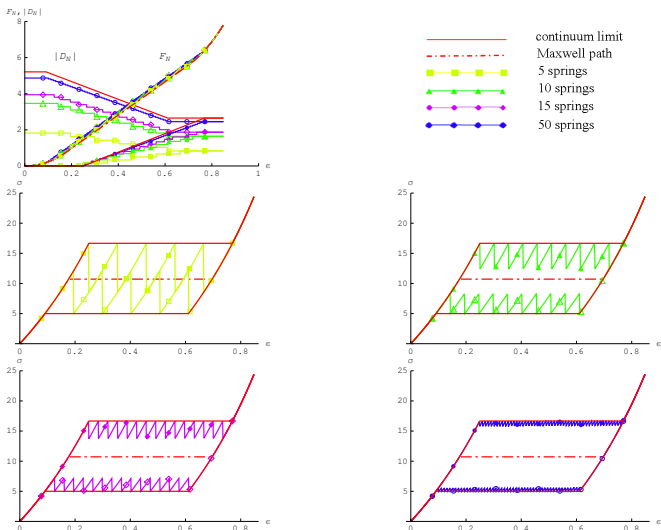
We examined uniform chains with fixed length $L = 860 \mu\text{m}$ and increasing number of microscopic springs N , subject to a complete loading-unloading compression cycle up to a global strain $\varepsilon = 0.85$. We assumed $k_c = k_0$ ('symmetric' case).

The numerical converged study confirmed the theoretical analysis concerned with the micro-meso transition.

We indeed numerically obtained overall stress-strain responses, which alternate elastic steps and 'plastic' jumps of σ at constant ε , and asymptotically converge to a 'perfectly plastic' behavior for $N \rightarrow \infty$.

Convergence study

Simulation of experimental results on compressed CNT foams



Simulation of experimental results on compressed CNT foams

We examined the experimental results of a compression test on a doubly anchored CNT foam run at the Graduate Aerospace Laboratories of the California Institute of Technology, and available literature results of cyclic compression tests on a foam-like CNT film (Cao et al., 2005).

We fitted the mechanical parameters of finite series of mesoscopic springs through Genetic Algorithms, which are well suited for global non-convex optimization.

Each examined experimental result consisted of a data set of the form

$$\left\{ \left\{ \varepsilon_r - \varepsilon_0, \bar{\sigma}_r \right\}_{r=1, \dots, N_d} \right\},$$

where

- ε_r : experimental observations of the global strain ε (hard-device tests)
- ε_0 : permanent strain eventually accumulated during a previous load history (mechanical preconditioning)
- $\bar{\sigma}_r$: experimental recordings of the overall stress σ
- N_d : number of data points

We sought the best-fit values of the constitutive parameters

$$\mathbf{p} = \left\{ \left\{ k_0^i, \Delta\sigma^i, k_c^i, \varepsilon_i^a, \varepsilon_c^i \right\}_{i=1, \dots, N-1} \right\}$$

under simple bounds of the form

$$\mathbf{p} \in D = [p_1^{lb}, p_1^{ub}] \times \dots \times [p_P^{lb}, p_P^{ub}]$$

upon prescribing the ratios k_{h+}^i/k_0^i and k_{h-}^i/k_0^i .

The fitting performance of a given set of parameters \mathbf{p} was evaluated through the fitting fitness function

$$f(\mathbf{p}) = \max_{r=1, \dots, N_d} |\sigma_r(\mathbf{p}) - \bar{\sigma}_r| \quad (4)$$

We employed a Breeder Genetic Algorithm (BGA) with a population size of $2P$ individuals; an initial, randomly-chosen, truncation rate equal to 15%, extended intermediate recombination, mutation rate in the interval [10%, 50%], and a maximum number of generations equal to 200.

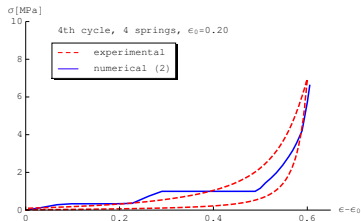
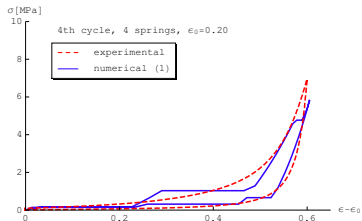
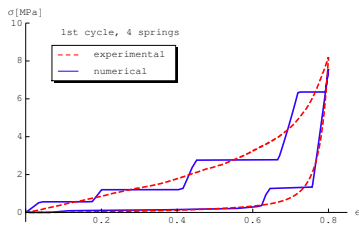
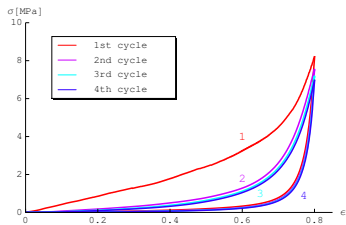
Simulation of compression tests on a doubly anchored CNT foam

We grew vertically aligned multi-walled carbon nanotube forests ($800\mu m$ in length with sample area $\sim 14mm^2$) by chemical vapor deposition (CVD). The average diameter of the as grown CNTs was $\sim 50nm$.

For anchoring the CNT-foams on a substrate, we spin-coated polydimethylsiloxane (PDMS) on top of a glass slide. Before curing the polymer we partially embedded the CNT-foams at $80^\circ C$ for 1 hour. After curing, the carbon nanotubes protruding from the substrate showed excellent vertical alignment with an average height of $\sim 750\mu m$.

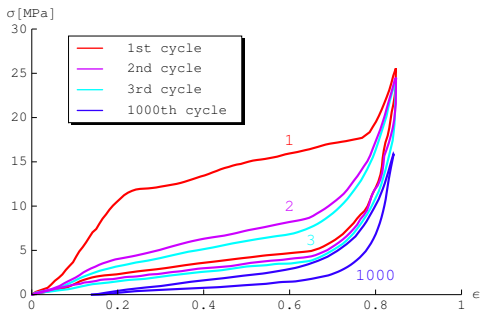
The process was repeated turning the sample upside down to obtain a 'doubly anchored' system (i.e. sandwich structure with polymer on both sides and the CNT foam in the middle).

Comparison between best-fit and experimental overall stress-strain curves

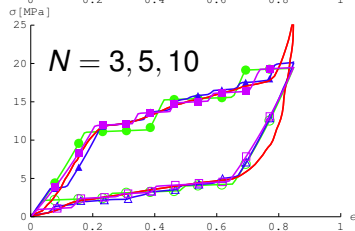
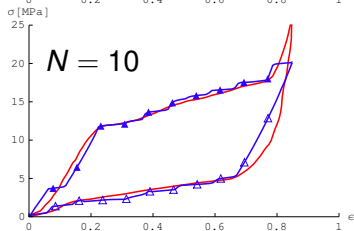
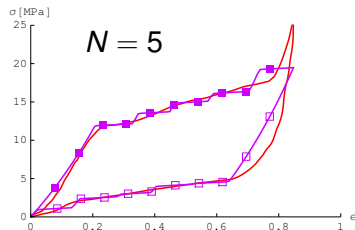
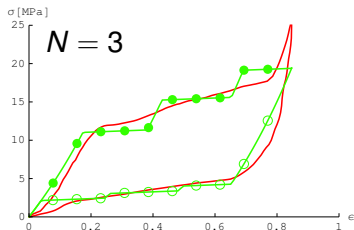


Fitting of cyclic compression tests on a foamlike CNT film

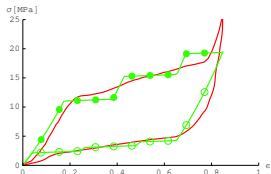
We fit a cyclic compression test given in Cao et al., 2005 for a CNT foamlike film with thickness $L = 860 \mu\text{m}$. The analyzed experiment performed 1000 loading/unloading cycles up to a global strain $\varepsilon = 0.85$



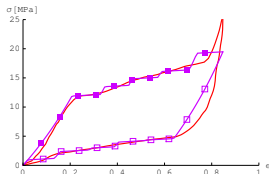
● Best-fit stress-strain curves: 'Symmetric' case ($k_c^i = k_0^i$)



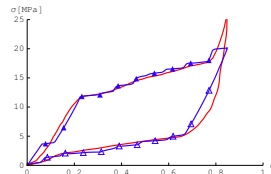
Deformation histories



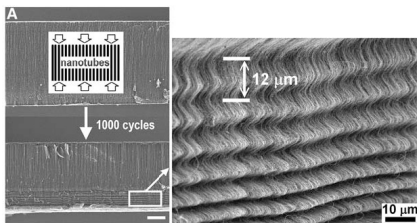
$N = 3$ movie >



$N = 5$ movie >

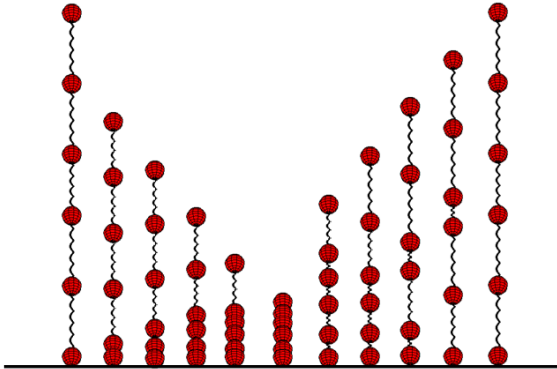


$N = 10$ movie >



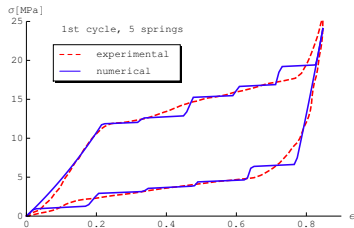
SEM of an original freestanding CNT foam-like film with thickness $860 \mu\text{m}$ (from Cao et al, Science, 2005)

Selected equilibrium configurations for $N = 5$

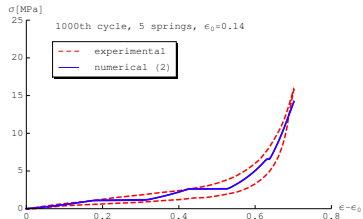
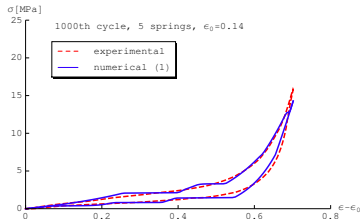
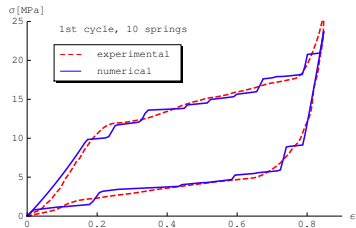


● Best-fit stress-strain curves: 'Asymmetric' case ($k_c^i \neq k_0^i$)

movie >



movie >



Multilayer CNT structures

We now pass to model the mechanics of a multilayer CNT structure through a lattice of mesoscopic springs, supposing that each spring represents a single layer, groups of layers, or portions of individual layers.

Such a simplified modelling implicitly assumes the interlayers between CNT arrays are as consistent and as negligible in their mechanical effects as possible, allowing for a clearer picture of the CNT mechanics.

In addition, we identify the material parameters of the multilayer structure through an '*in-situ*' procedure, which is founded upon the experimental characterisation of the local deformation of the tubes.

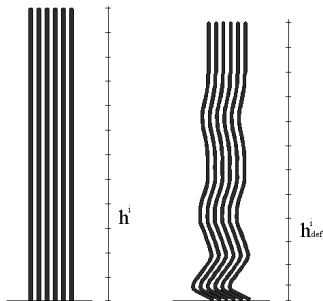
The proposed identification procedure requires an experimental apparatus that allows the characterisation of the CNT morphology alongside the load-displacement curve (e.g., by using a high resolution CCD camera, or a scanning electron microscope).

In hard-device conditions, the order parameter of a quasi-static compression test will be the global strain ε , and the stress σ will be approximatively constant along the thickness of the structure.

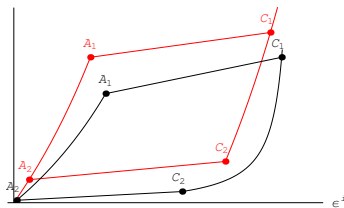
Frames taken from an *in situ* video of the experiment can be used to track the local deformation of vertical portions (or segments) S^i of the CNT structure ($i = 1, \dots, N$).

An approximation to the local strain ε^i of \mathcal{S}^i is given by $(h^i - h_{def}^i)/h^i$.

$$\varepsilon^i \approx \frac{h^i - h_{def}^i}{h^i}$$



With reference to the generic element \mathcal{S}^i , we identify the point denoted by A_1 with the state immediately preceding the snap-buckling of such a portion of the structure, as determined through inspection of the frames forming the video recording of the experiment. Similarly, we identify C_1 with the state marking the beginning of the final densification phase; and C_2 with the state immediately preceding the local snap-back of the CNTs to an unbuckled state.



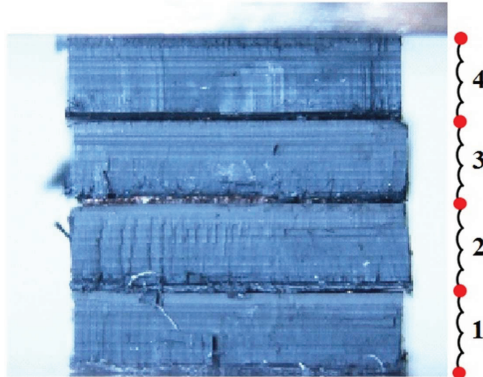
Estimation of the mechanical parameters of a four-layer structure

We estimated the material parameters of a four-layer structure composed of alternating layers of multi-walled CNTs and copper tape, under quasi-static compression tests up to the total strain $\varepsilon = 0.4$,

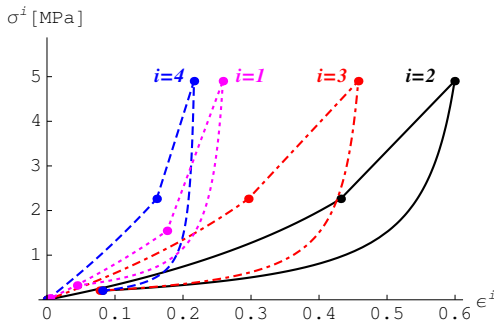
We constructed two different mass-spring models of such a structure, through the *in situ* identification procedure (Models # 1 and # 2), which were composed of 4 and 3 springs, respectively.

Subsequently, we refined the properties of the above models through BGA optimisation, obtaining the best-fit Models # 3 (4 springs) and # 4 (3 springs).

Four-spring model



A four spring scheme, in which each spring represents exactly one CNT layer, is used for Models # 1 and #2.

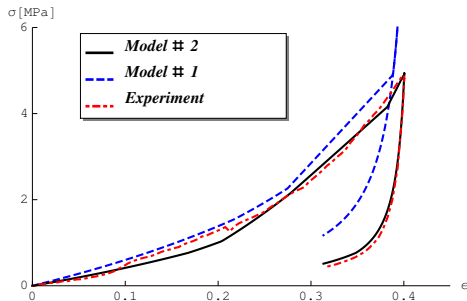


In situ identification of the stress-strain curves of the four springs forming Model # 1.

The bulk densities for the middle two layers of the examined structure were less than those for the top and bottom layers. Thus the increased stiffness of the top and bottom springs forming Model # 1, as compared to that of the terminal layers, is in agreement with the distribution of the bulk density.

In the present case, most of the theory-experiment deviation is localised in a very narrow region corresponding to the final portion of the densification regime ($\varepsilon \geq 0.35$).

A BGA optimisation of Model # 1 (fitting performance $f = 1.19$ MPa) led to the best-fit Model # 2, which shows fitting performance $f = 0.13$ MPa.

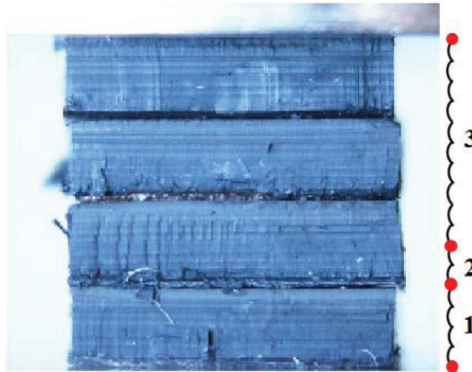


Comparison between the overall stress-strain curves predicted by Models # 1 and # 2, and the recorded experimental response.

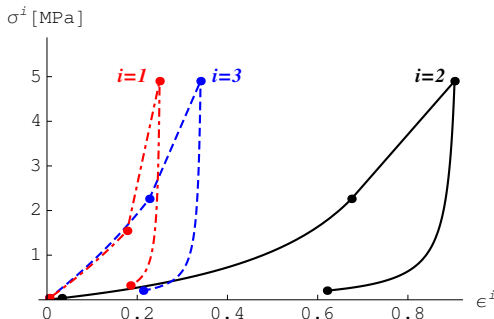
Three-spring model

As previously mentioned, the largest deformation of the CNT structure collapse was observed in experiments at the bottom of layer # 2.

To design a model that would capture more closely the experimental observations, we constructed a three-spring model in which one spring was placed in correspondence with the heavily buckled region, and two other springs modelled the behaviour of the remaining portions of the material below and above the deformed region.



A three spring scheme is used for Models # 3 and # 4.



In situ identification of the stress-strain curves of the three springs forming Model # 3.

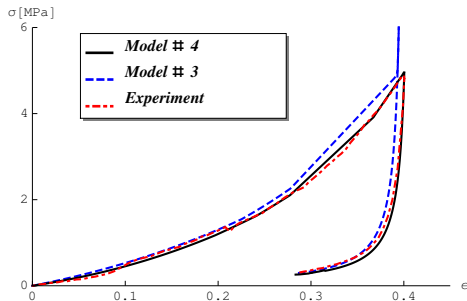


Fig. 1: Comparison between the overall stress-strain curves predicted by Models # 3 and # 4, and the recorded experimental response.

Fig. 1 shows a good agreement between the overall σ vs ε response predicted by Model # 3 and the corresponding experimental response, with fitting performance $f = 1.15$ MPa.

A BGA optimisation of Model #3 led to the response denoted as Model #4 in Fig. 1, which shows an excellent agreement with the experimental one and fitting performance $f = 0.09$ MPa.

Selected frames from the videos for the experiment and the response of Model # 4 are shown in Fig. 2.

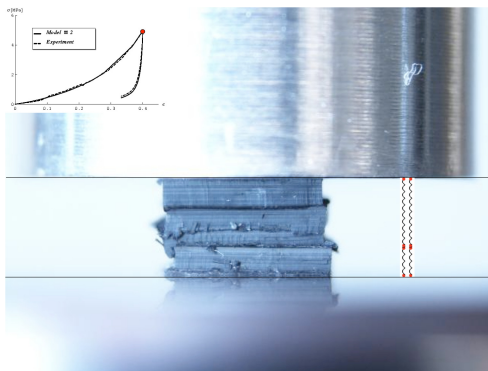


Fig. 2: Comparison between frames from the videos for the experiment and the response of Model # 4, for different values of the overall strain ϵ .

Mechanical modeling of CNT structures

Part III: Conclusions and future work

Fernando Fraternali
University of Salerno

Workshop
Carbon nanotubes as components in bulk materials
University of Salerno
October 25 - November 04, 2011

1 Conclusions

2 Future work

- A common variational framework for bio- and nano-structures
- Information-passing approaches
- Experimental parameter identification

Conclusions 1/6

The results concerned with nanostructures have led us to the first extension to-date of mass-spring models with bistable springs to the multiscale mechanical modelling of carbon nanotube assemblies.

We have developed a mesoscopic model that predicts time-independent hysteresis of such structures through the succession of snapping events at the microscopic scale.

The latter mimic local collapse of the tubes due to the enucleation and propagation of local buckling phenomena (Cao et al., 2005; Hutchens et al., 2010) and explain energy dissipation in the form of 'transformational' plasticity (Puglisi and Truskinovsky, 2005).

Conclusions 2/6

The proposed model differs from other bistable mass-spring models available in the literature, due to the presence of an intermediate, mesoscopic scale, placed in between the microscopic scale of the bistable springs, and the macroscopic scale of the overall structure.

The microscopic scale aims to describe the dynamic snapping of the carbon nanotubes, due to local buckling, while the mesoscopic scale is intended to describe the time-independent hysteretic behaviour of finite portions of the CNT foam, through the concept of 'transformational' plasticity (Puglisi and Truskinovsky, 2005). The hysteresis typically follows from kinking, sticking and entanglement of the tubes, friction and other microscopic dissipative effects.

Conclusions 3/6

Another relevant difference between the present model and most of the available bistable mass-spring models consists of the fact that the current model accounts for nonuniform mesoscopic spring properties, while other models usually consider uniform chains of bistable springs.

Such a mechanical inhomogeneity allows us to account for hardening of the macroscopic response in the post-buckling range.

The fitting of experimental stress-strain curves allowed us to recognise that non-uniform, dissipative mass-spring models are well suited to capture the main features of the real compressive response of CNT foams, and specifically strain localisation due to CNT kinking and time-independent hysteresis.

Conclusions 4/6

In particular, the energy dissipation ability of CNT foams was found to be relevant during loading/unloading from the pristine state, and progressively decaying after mechanical preconditioning. By setting to zero the dissipation of the model, we were led to obtain a rough, non-linearly elastic approximation of the examined experimental behaviours after preconditioning.

We have extended the mechanical modeling of CNT foams to the case of multilayer composites based on alternating layers of aligned CNTs and anchoring foils. To this aim, we have proposed a simplified modelling, which supposes that each mesoscopic dissipative element may represent either a single layer, or a suitably chosen different portion of the structure.

Conclusions 5/6

We have also presented an *in situ* identification procedure, which allows one to obtain the mechanical properties of the different springs forming the proposed models, through experimental characterisation of local deformation of the aligned CNTs alongside a given load-displacement curve.

We applied the model to characterise the mechanical response of a four-layer CNT structure, tracking the local deformation of the layers under compression.

We observed that the proposed procedure is able to produce a good approximation of the experimental response, capturing its main features and reproducing the localisation of the buckling deformation.

Conclusions 6/6

The *in situ* identified model can be usefully refined through a successive GA optimisation of material parameters.

Experimental observations have shown that, within an individual layer of aligned CNTs under compression, buckling always begins on the side nearest the substrate, resulting in the localisation of strain in this region (Cao et al., 2005; Misra et al. 2010; Hutchens et al., 2010).

Taking into account the above observations and accurately analysing the dynamics of the experiment on hand, we showed that it is possible to perform an optimal choice of the fitting model (number and localisation of the springs), which significantly improves the theory-experiment matching.

Future work

A common variational framework for nanostructures

We plan to develop a database of multiscale models to be applied to a variety of engineering nanostructures.

This will imply the determination of the continuum limits of the interaction potentials characterising such structures, which include bond, dihedral angle, bistable spring and Lennard-Jones type interactions, and the analysis of hexagonal and/or cubic geometries.

We intend to examine 2D and/or 3D particle assemblies and study their mesoscopic response through experimental, mathematical, and numerical arguments.

Future work

Information-passing approaches

The outcomes of this study can be usefully employed to develop an information-passing multiscale modelling of nanoparticle networks.

As a matter of fact, the prediction of mesoscopic limiting energies and stress-strain relationships from discrete elements/molecular dynamics simulations, eventually different from region to region of the model, allows one to adequately inform simulations at the continuum scale.

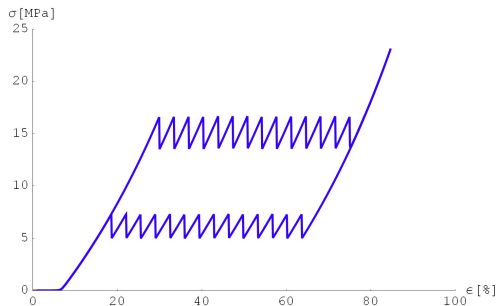
We plan to develop analytical formulae for standard geometries, predicting the effects of stretching strains, curvatures, and microscopic phase-transitions on the mesoscopic response.

Future work

New physical challenges

The inclusion of permanent deformation in the proposed models is rather straightforward and can be carried out by 'freezing' the response of selected springs. Rate-dependent effects and van der Waals forces can also be modelled by suitably adding dashpots and long-range springs to the discrete model.

Other targets of the present models are multilayer CNT structures with polymer interlayers; complex multilayer composite structures in which aligned CNTs can be partially or fully embedded in various polymeric matrices; phononic crystals; and periodic microporous structures (Srikanth et al., 2009; Jang et al., 2009).



movie > Modeling of permanent deformation by setting to zero the stiffness of a microscopic spring.

Future work

Experimental parameter identification

We also plan to develop a multiscale *in-situ* identification of the bistable spring models here presented, by combining experimental observations of the local CNT deformation through SEM (microscopic response) and high resolution cameras (mesoscopic response).

In particular, observations at the microscopic scale, performed e.g. through the SEMentor equipment described in Hutchens et al. (2010), could lead to an improved ‘micromechanical’ validation of the bistable spring model for CNT arrays, proving the correspondence between stress ‘humps’ in the overall response and local buckling of the tubes.